Measurement of the shape of the $\Lambda_b^0 \to \Lambda_c^+ \mu^- \bar{\nu}_\mu$ differential decay rate

R. Aaij *et al.*[*]

(LHCb Collaboration)

A measurement of the shape of the differential decay rate and the associated Isgur-Wise function for the decay $\Lambda_b^0 \to \Lambda_c^+ \mu^- \bar{\nu}_\mu$ is reported, using data corresponding to 3 fb^{-1} collected with the LHCb detector in proton-proton collisions. The $\Lambda_c^+ \mu^- \bar{\nu}_\mu$(+anything) final states are reconstructed through the detection of a muon and a Λ_c^+ baryon decaying into $pK^-\pi^+$, and the decays $\Lambda_b^0 \to \Lambda_c^+ \pi^+ \pi^- \mu^- \bar{\nu}_\mu$ are used to determine contributions from $\Lambda_b^0 \to \Lambda_c^{*+} \mu^- \bar{\nu}_\mu$ decays. The measured dependence of the differential decay rate upon the squared four-momentum transfer between the heavy baryons, q^2, is compared with expectations from heavy-quark effective theory and from unquenched lattice QCD predictions.

I. INTRODUCTION

In the Standard Model (SM) of particle physics, quarks participate in a rich pattern of flavor-changing transitions. The relevant couplings form a complex 3×3 matrix, known as the Cabibbo-Kobayashi-Maskawa (CKM) matrix, characterized by just four independent parameters [1]. A vast body of measurements of individual CKM elements exists, and thus the overall consistency of the SM picture of charged current interactions is highly overconstrained. Decades of experimental work have demonstrated the impressive consistency of experimental data with the CKM paradigm [2,3]; nonetheless, the motivation to probe the CKM matrix remains strong. Effects of physics beyond the SM may be subtle; thus, more precise measurements are necessary to unveil them. Semileptonic decays of heavy-flavored hadrons are commonly used to measure CKM parameters, as they involve only one hadronic current, parametrized in terms of scalar functions known as form factors. The number of form factors needed to describe a particular decay depends upon the spin of the initial- and final-state hadrons [4,5]. A precise calculation of these form factors has been elusive for many years as it is not possible in perturbative QCD. Heavy-Quark Effective Theory (HQET) provides the framework to systematically include nonperturbative corrections in computations involving hadrons containing heavy quarks. In particular, in the limit of infinite heavy-quark mass, all the form factors describing the semileptonic decay of a heavy-flavored hadron are proportional to a universal function, known as the Isgur-Wise (IW) function [6]. Lattice QCD,

namely the use of lattice formulations of QCD in large scale numerical simulations, has emerged in recent years as a technique with well-defined and systematically improvable uncertainties which can be applied to a wide range of processes and physical quantities [7]. Predictions from the infinite heavy-quark mass limit are useful as a check of several lattice QCD calculations [8].

The decay $\Lambda_b^0 \to \Lambda_c^+ \mu^- \bar{\nu}_\mu$ is described by six form factors corresponding to the vector and axial-vector components of the flavor-changing charged current [9]. In HQET, Λ_b^0 decays are particularly simple, as the light ud quark pair has total spin $j = 0$, and thus the chromomagnetic corrections, which are of the order of a few percent for B mesons, are not present [10]. In the static approximation of infinite heavy-quark masses, the six form factors characterizing the baryonic semileptonic decay[1] $\Lambda_b^0 \to \Lambda_c^+ \mu^- \bar{\nu}_\mu$ can be expressed in terms of the elastic heavy-baryon Isgur-Wise function $\xi_B(w)$ [11]. The scalar invariant $w \equiv v_{\Lambda_b^0} \cdot v_{\Lambda_c^+}$ is related to the squared four-momentum transfer between the heavy baryons, q^2, by

$$w = (m_{\Lambda_b^0}^2 + m_{\Lambda_c^+}^2 - q^2)/(2m_{\Lambda_b^0} m_{\Lambda_c^+}), \qquad (1)$$

where $v_{\Lambda_b^0}$ and $v_{\Lambda_c^+}$ are the four-velocities of the Λ_b^0 and Λ_c^+ baryons, respectively, and $m_{\Lambda_b^0}$ and $m_{\Lambda_c^+}$ are the corresponding invariant masses. Nonperturbative corrections to the static limit can be expressed in terms of an expansion in powers of $1/m_c$ and $1/m_b$, where m_c and m_b represent the c- and b-quark masses, respectively. It has been shown in Ref. [12] that the $1/m_c$ term can be expressed in terms of $\xi_B(w)$ and one dimensionful constant. Moreover, partial cancellations lead to small first-order corrections near $w = 1$ [13].

---

[*]Full author list given at the end of the article.

---

[1]The inclusion of charge-conjugate modes is implied throughout this paper.

In the static approximation, the differential decay width of the $\Lambda_b^0 \to \Lambda_c^+ \mu^- \bar{\nu}_\mu$ decay is given by

$$\frac{d\Gamma}{dw} = GK(w)\xi_B^2(w), \qquad (2)$$

where the constant factor G is given by

$$G = \frac{2}{3}\frac{G_F^2}{(2\pi)^3}|V_{cb}|^2(m_{\Lambda_b^0})^4 r^2 \quad \text{with} \quad r = m_{\Lambda_c^+}/m_{\Lambda_b^0}, \qquad (3)$$

where G_F represents the Fermi coupling constant [14], $|V_{cb}|$ is the magnitude of the matrix element describing the coupling of the c quark to the b quark, and the kinematic factor $K(w)$ is given by

$$K(w) = m_{\Lambda_c^+}\sqrt{w^2 - 1}[3w(1 - 2rw + r^2) + 2r(w^2 - 1)]. \qquad (4)$$

The function $\xi_B(w)$ cannot be determined from first principles in HQET, but calculations based on a variety of approaches exist. The kinematic limit $w = 1$ is special in HQET, as only modest corrections in the $(1/m_b, 1/m_c)$ expansion are expected, due to the absence of hyperfine corrections [15]. Thus, it is interesting to express ξ_B as a Taylor series expansion

$$\xi_B(w) = 1 - \rho^2(w - 1) + \frac{1}{2}\sigma^2(w - 1)^2 + \cdots, \qquad (5)$$

where ρ^2 is the magnitude of the slope of ξ_B and σ^2 is its curvature at $w = 1$. Sum rules provide constraints on ρ^2 and σ^2. In particular, they require the slope at the zero recoil point to be negative and give bounds on the curvature and higher-order derivatives [16,17]. In addition, they predict $\sigma^2 \geq 3/5[\rho^2 + (\rho^2)^2]$ [18] and $\rho^2 \geq 3/4$. Table I summarizes theoretical predictions for ρ^2 from quenched lattice QCD, QCD sum rules, and a relativistic quark model.

Recently, state-of-the-art calculations of the six form factors describing the decay $\Lambda_b^0 \to \Lambda_c^+ \mu^- \bar{\nu}_\mu$ have been obtained using lattice QCD with $2 + 1$ flavors of dynamical domain-wall fermions [19]. These form factors are calculated in terms of q^2. More details on this formalism are given in Appendix A. The resulting theoretical uncertainty attached to a measurement of $|V_{cb}|$ using this form-factor prediction is about 3.2%. The precision of this calculation makes this approach an appealing alternative to the ones currently used, all based on B-meson semileptonic decays such as $\bar{B}^0 \to D^{*+}\mu^-\bar{\nu}_\mu$. Thus, it is important to examine the model's agreement with measured quantities such as the shape of the $d\Gamma/dq^2$ spectrum.

The experimental knowledge of Λ_b^0 semileptonic decays is quite sparse, as this baryon is too heavy to be produced at the e^+e^- B-factories. The only previous experimental study of $\xi_B(w)$ was performed by the DELPHI experiment at

TABLE I. Predictions for the slope at zero recoil of the baryonic Isgur-Wise function ξ_B. The evaluation from Ref. [21] includes first-order corrections in HQET.

ρ^2	Approach	Reference
1.35 ± 0.13	QCD sum rules	[22]
$1.2^{+0.8}_{-1.1}$	Lattice QCD (static approximation)	[23]
1.51	HQET + relativistic wave function	[21]

LEP, which obtained $\rho^2 = 2.03 \pm 0.46(\text{stat})^{+0.72}_{-1.00}(\text{syst})$, with an overall uncertainty of the order of 50% [20].

In this paper, we describe a determination of the shape of the w or q^2 spectrum of the decay $\Lambda_b^0 \to \Lambda_c^+ \mu^- \bar{\nu}_\mu$ and compare it with functional forms related to a single form factor, inspired by HQET, and the lattice QCD prediction of Ref. [19]. Section II presents the experimental procedure and simulated samples, while Sec. III describes the method employed to reconstruct $\Lambda_b^0 \to \Lambda_c^+ \mu^- \bar{\nu}_\mu$ candidates and to estimate the corresponding kinematic variables w and q^2. Section IV describes the method adopted to isolate the signal, the unfolding procedure used to account for experimental resolution effects, and the efficiency corrections. The fit results for $\xi_B(w)$ corresponding to different functional forms are summarized in Sec. V. The same analysis procedure is used in Sec. VI to derive the shape of the differential decay width $d\Gamma/dq^2(\Lambda_b^0 \to \Lambda_c^+ \mu^- \bar{\nu}_\mu)$ and compare with the predictions of Ref. [19]. These data are also fitted with a single form-factor parametrization that corresponds to the HQET infinite heavy-quark mass limit.

II. EXPERIMENTAL METHOD

The data used in this analysis were collected with the LHCb detector at the Large Hadron Collider at CERN and correspond to 1 fb^{-1} of integrated luminosity collected at a center-of-mass energy of 7 TeV in 2011 and 2 fb^{-1} collected at a center-of-mass energy of 8 TeV in 2012.

The LHCb detector [24,25] is a single-arm forward spectrometer designed for the study of particles containing b or c quarks. The detector covers the pseudorapidity range $2 < \eta < 5$, where η is defined in terms of the polar angle θ with respect to the beam direction as $-\ln(\tan \theta/2)$. The detector includes a high-precision tracking system consisting of a silicon-strip vertex detector surrounding the pp interaction region [26], a large-area silicon-strip detector located upstream of a dipole magnet with a bending power of about 4 Tm, and three stations of silicon-strip detectors and straw drift tubes [27] placed downstream of the magnet. The tracking system provides a measurement of the momentum, p, of charged particles with a relative uncertainty that varies from 0.5% at low momentum to 1.0% at 200 GeV.[2] The minimum distance of a track to a

---

[2]Natural units with $c = \hbar = 1$ are used throughout.

primary vertex, the impact parameter (IP), is measured with a resolution of $(15 + 29/p_T)$ μm, where p_T is the component of the momentum transverse to the beam, in GeV. Different types of charged hadrons are distinguished using information from two ring-imaging Cherenkov detectors (RICH) [28]. Photons, electrons, and hadrons are identified by a calorimeter system consisting of scintillating-pad and preshower detectors, an electromagnetic calorimeter, and a hadronic calorimeter. Muons are identified by a system composed of alternating layers of iron and multiwire proportional chambers [29]. The online event selection is performed by a trigger [30], which consists of a hardware stage, based on information from the calorimeter and muon systems, followed by a software stage, which applies a full event reconstruction.

Muon candidates are first required to pass the hardware trigger that selects muons with a transverse momentum $p_T > 1.6$ (1.8) GeV for the 2011 (2012) data taking period. In the subsequent software trigger, events with one particle identified as a muon are selected if at least one of the final-state particles has both $p_T > 0.8$ GeV and IP larger than 100 μm with respect to all of the primary pp interaction vertices (PVs) in the event. In the offline selection, trigger signals are associated with reconstructed particles. Selection requirements can therefore be made on the trigger selection itself and on whether the decision was due to the signal candidate, other particles produced in the pp collision, or a combination of both. This classification of trigger selections can be used for data-driven efficiency determination. Finally, the tracks of two or more of the final-state particles are required to form a vertex that is significantly displaced from the PVs.

Our study makes use of simulated semileptonic decays, where pp collisions are generated using PYTHIA [31] with a specific LHCb configuration [32]. Decays of hadronic particles are described by EvtGen [33], in which final-state radiation is generated using PHOTOS [34]. The interaction of the generated particles with the detector, and its response, are implemented using the GEANT4 toolkit [35] as described in Ref. [36].

III. EVENT RECONSTRUCTION

To isolate a sample of $\Lambda_b^0 \to \Lambda_c^+ \mu^- \bar{\nu}_\mu X$ semileptonic decays, where X represents the undetected particles produced with the Λ_c^+ in the c-quark hadronization, we combine $\Lambda_c^+ \to pK^-\pi^+$ candidates with tracks identified as muons. We consider candidates where a well-identified muon passing the hardware and software trigger algorithms with momentum greater than 3 GeV is found. Charmed baryon candidates are formed from hadrons with momenta greater than 2 GeV and transverse momenta greater than 0.3 GeV. In addition, we require that the average of the magnitudes of the transverse momenta of the hadrons forming the Λ_c^+ candidate be greater than 0.7 GeV. Kaons, pions, and protons are identified using the RICH system. Each track's IP

significance with respect to the associated primary vertex is required to be greater than 9.[3] Moreover, the selected tracks must be consistent with coming from a common vertex: the χ^2 per degree of freedom (χ^2/DOF) of the vertex fit must be smaller than 6. In order to ensure that the direction of the parent Λ_b^0 is well measured, the Λ_c^+ vertex must be distinct from the primary pp interaction vertex. To this end, we require that the flight-distance significance of the Λ_c^+ candidate (defined as the measured flight distance divided by its uncertainty) with respect to the associated PV be greater than 100.

Partially reconstructed Λ_b^0 baryon candidates are formed combining μ^- and Λ_c^+ candidates that are consistent with coming from a common vertex, and we require that the angle between the direction of the momentum of the $\Lambda_c^+ \mu^-$ candidate and the line from the associated PV to the $\Lambda_c^+ \mu^-$ vertex be less than 45 mrad. As the Λ_c^+ baryon is a Λ_b^0 decay product with a small but significant lifetime, we require that the difference in the component of the decay vertex position of the charmed hadron candidate along the beam axis and that of the beauty candidate be positive. We explicitly require that the Λ_b^0 hadron candidate pseudorapidity be between 2 and 5. We measure η using the line defined by connecting the associated PV and the vertex formed by the Λ_c^+ and the μ^- lepton. Finally, the invariant mass of the $\Lambda_c^+ \mu^-$ system must be between 3.3 and 5.3 GeV. These selection criteria ensure that the Λ_c^+ candidates are decay products of Λ_b^0 semileptonic decays. In particular, the background from directly produced Λ_c^+ (prompt Λ_c^+) is highly suppressed. This is quantified by an unbinned extended maximum likelihood fit to the two-dimensional $pK^-\pi^+$ invariant mass and ln(IP/mm) distributions of the Λ_c^+ candidates, where "/mm" refers to the length unit used to measure the IP. The ln(IP/mm) component allows us to determine the small prompt Λ_c^+ background. The parameters of the IP distribution of the prompt sample are found by examining directly produced charm hadrons, as described in Ref. [37]. An empirical probability density function (PDF) derived from simulation is used for the Λ_c^+ from Λ_b^0 component. We find $(2.74 \pm 0.02) \times 10^6$ $\Lambda_c^+ \to pK^-\pi^+$ candidates, which can be interpreted as $\Lambda_b^0 \to \Lambda_c^+ \mu^- \bar{\nu}_\mu X$ decays, and we determine the prompt $\Lambda_c^+ \to pK^-\pi^+$ fraction to be 1.5%, which can be neglected. The corresponding fit is shown in Fig. 1.

Our goal is the study of the ground-state semileptonic decay $\Lambda_b^0 \to \Lambda_c^+ \mu^- \bar{\nu}_\mu$; thus, we need to estimate the contributions from Λ_c^{*+} decaying into $\Lambda_c^+ \pi\pi$ states. Theoretical predictions suggest that the inclusive rate $\Lambda_b^0 \to \Lambda_c^+ \mu^- \bar{\nu}_\mu X$ is dominated by the exclusive channel $\Lambda_b^0 \to \Lambda_c^+ \mu^- \bar{\nu}_\mu$ [38,39]. The residual contribution is expected to be accounted for by

---

[3]The associated primary vertex to a $\Lambda_b^0 \to \Lambda_c^+ \mu^- \bar{\nu}_\mu X$ candidate is selected as the primary vertex which minimizes the IP significance of the $\Lambda_c^+ \mu^-$ system.
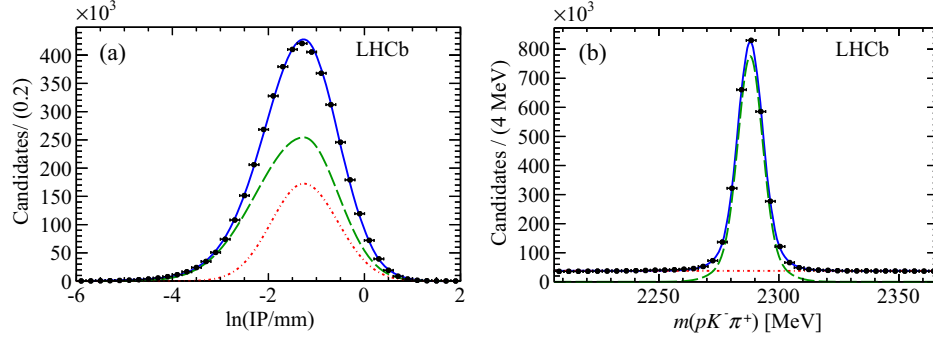
FIG. 1. (a) The ln(IP/mm) distribution and (b) $pK^-\pi^+$ invariant mass for Λ_c^+ candidate combinations with a muon. The red (dashed-dotted) curves show the combinatorial Λ_c^+ background, the green (dashed) curves show the Λ_c^+ from Λ_b^0, and the blue-solid curves show the total yields.

the $\Lambda_b^0 \to \Lambda_c(2595)^+\mu^-\bar{\nu}_\mu$ and $\Lambda_b^0 \to \Lambda_c(2625)^+\mu^-\bar{\nu}_\mu$ channels. Other modes, such as $\Lambda_b^0 \to \Sigma_c^+\mu^-\bar{\nu}_\mu$, are suppressed in the static limit and to order $1/m_Q$, where m_Q represents the heavy-quark mass (m_c or m_b) [40], with an additional stronger suppression factor of the order $(m_d - m_u)/m_c$ rather than $(m_d - m_u)/m_{\Lambda_{QCD}}$ [9].

We use $\Lambda_b^0 \to \Lambda_c^+\pi^+\pi^-\mu^-\bar{\nu}_\mu$ decays to infer contributions from the excited Λ_c^+ modes, where the Λ_c^+ candidates are selected as $pK^-\pi^+$ combinations of which the invariant mass is within ±20 MeV of the nominal Λ_c^+ mass. The $\Lambda_c^+\mu^-\bar{\nu}_\mu$ candidates are combined with pairs of opposite-charge pions that satisfy criteria similar to those used to select the pions from the Λ_c^+ decay. The minimum transverse momentum of these pions is required to be 0.2 GeV, and the transverse momentum of the $\Lambda_c^+\pi^+\pi^-$ system is required to be greater than 1.5 GeV. Lastly, the χ^2 per degree of freedom of the vertex fit for the $\Lambda_c^+\pi^+\pi^-$ system must be smaller than 6.

The resulting spectrum, measured as the mass difference $m(pK^-\pi^+\pi^-\pi^+) - m(pK^-\pi^+)$ added to the known Λ_c^+ mass [14], is shown in Fig. 2. We see peaks corresponding to the $\Lambda_c(2595)^+$, $\Lambda_c(2625)^+$, $\Lambda_c(2765)^+$, and $\Lambda_c(2880)^+$

resonances. The $\Lambda_c(2595)^+$ is only a few MeV above the kinematic threshold, and thus it is not well described by a Breit-Wigner function. The baseline fit for this resonance uses a PDF consisting of the sum of two bifurcated Gaussian functions. As a check, we use an S-wave relativistic Breit-Wigner convolved with a Gaussian function with standard deviation $\sigma = 2$ MeV that accounts for the detector resolution. While the second parametrization is more accurate, the fits to the invariant mass spectra in different kinematic bins are more stable with the baseline parametrization. We fit the $\Lambda_c(2625)^+$ signal with a double Gaussian PDF with shared mean, as the natural width is expected to be well below the measured detector resolution. The shape of the combinatoric background PDF is inferred from wrong-sign (WS) candidates, where a $\pi^+\pi^+$ or $\pi^-\pi^-$ pair is combined with Λ_c^+ instead of $\pi^+\pi^-$. In addition, we observe peaks corresponding to two higher-mass resonances, with masses and widths consistent with the $\Lambda_c(2765)^+$ and $\Lambda_c(2880)^+$ baryons [14]. In order to determine their yields, we fit the two signal peaks with single Gaussian PDFs with unconstrained masses and widths. The measured yields for the four Λ_c^+ final states, as well as the $\Lambda_c^+\mu^-\bar{\nu}_\mu X$ final state, are presented in Table II.
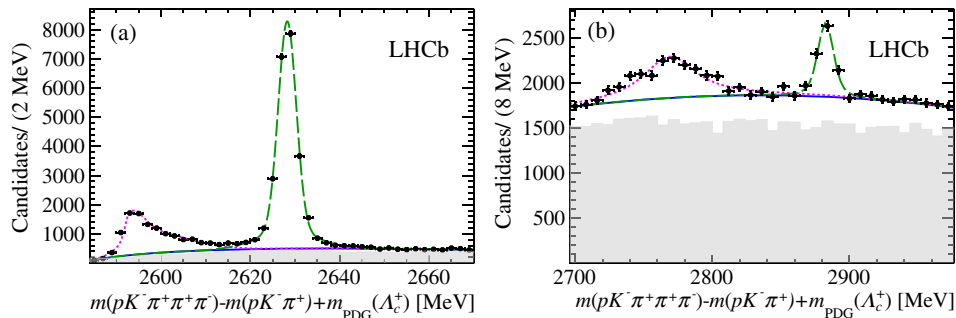

FIG. 2. The mass difference $m(pK^-\pi^+\pi^+\pi^-) - m(pK^-\pi^+)$ added to the known Λ_c^+ mass, $m_{PDG}(\Lambda_c^+)$ [14], for candidates with $pK^-\pi^+$ invariant mass within ±20 MeV of the known Λ_c^+ mass in candidate semileptonic decays for the entire w range: data are shown as black dots, the combinatoric background is shown as a blue solid line, and the gray histogram shows the WS spectrum, obtained by combining a $\pi^+\pi^+$ or $\pi^-\pi^-$ pair with Λ_c^+ instead of $\pi^+\pi^-$. The signal fits are identified as follows: (a) for $m < 2700$ MeV, the $\Lambda_c(2595)^+$ as a magenta dashed line and the $\Lambda_c(2625)^+$ as a green long-dashed line; (b) for $m > 2700$ MeV, the $\Lambda_c(2765)^+$ as a magenta dashed line and the $\Lambda_c(2880)^+$ as a green long-dashed line.

TABLE II. Measured raw yields for the four $\Lambda_c^{*+}\mu^-\bar{\nu}_\mu$ final states and the inclusive $\Lambda_c^+\mu^-\bar{\nu}_\mu X$.

Final state	Yield
$\Lambda_c(2595)^+\mu^-\bar{\nu}_\mu$	8569 ± 144
$\Lambda_c(2625)^+\mu^-\bar{\nu}_\mu$	22965 ± 266
$\Lambda_c(2765)^+\mu^-\bar{\nu}_\mu$	2975 ± 225
$\Lambda_c(2880)^+\mu^-\bar{\nu}_\mu$	1602 ± 95
$\Lambda_c^+\mu^-\bar{\nu}_\mu X$	$(2.74 \pm 0.02) \times 10^6$

The measured contributions from the two heavier Λ_c^{*+} final states, shown in Table II, are smaller than those from $\Lambda_b^0 \to \Lambda_c(2595)^+\mu^-\bar{\nu}_\mu$ and $\Lambda_b^0 \to \Lambda_c(2625)^+\mu^-\bar{\nu}_\mu$ decays. No theoretical prediction for nonresonant $\Lambda_b^0 \to \Lambda_c^+\pi^+\pi^-\mu^-\bar{\nu}_\mu X$ exists, but we estimate systematic uncertainties due to the subtraction of this component with an alternative fit of the $\Lambda_b^0 \to \Lambda_c^+\pi^+\pi^-\mu^-\bar{\nu}_\mu X$ spectrum from candidate Λ_b^0 semileptonic decays, where we derive both the yield and shape of the combinatoric background from the WS sample.

The kinematical quantities q^2 and w in the decay $\Lambda_b^0 \to \Lambda_c^+\mu^-\bar{\nu}_\mu$ can be calculated if the magnitude of the Λ_b^0 momentum is known. The Λ_b^0 flight direction can be inferred from the primary and secondary vertex locations, and this input, combined with the constraints from energy and momentum conservation, implies the following relationship for $p_{\Lambda_b^0}$,

$$\left[\left(\frac{\hat{p}_{\Lambda_b^0} \cdot \vec{p}_{\Lambda_c^+\mu^-}}{E_{\Lambda_c^+\mu^-}}\right)^2 - 1\right] p_{\Lambda_b^0}^2 + \left[(m_{\Lambda_b^0}^2 + m_{\Lambda_c^+\mu^-}^2)\frac{\hat{p}_{\Lambda_b^0} \cdot \vec{p}_{\Lambda_c^+\mu^-}}{E_{\Lambda_c^+\mu^-}^2}\right] p_{\Lambda_b^0}$$
$$+ \left[\left(\frac{(m_{\Lambda_b^0}^2 + m_{\Lambda_c^+\mu^-}^2)}{2E_{\Lambda_c^+\mu^-}}\right)^2 - m_{\Lambda_b^0}^2\right] = 0, \tag{6}$$

where the unit vector $\hat{p}_{\Lambda_b^0}$ is the direction of the Λ_b^0 baryon, $\vec{p}_{\Lambda_c^+\mu^-}$ is the momentum of the $\Lambda_c^+\mu^-$ pair, $E_{\Lambda_c^+\mu^-}$ is the energy of the $\Lambda_c^+\mu^-$ pair, $m_{\Lambda_c^+\mu^-}$ is the invariant mass of the $\Lambda_c^+\mu^-$ pair, $m_{\Lambda_b^0}$ is the nominal mass of the Λ_b^0 baryon, and Λ_c^+ identifies the $pK^-\pi^+$ combination. This is a quadratic equation, reflecting the lack of knowledge of the neutrino orientation in the Λ_b^0 rest frame with respect to the Λ_b^0 direction in the laboratory. The solution corresponding to the lower value of $p_{\Lambda_b^0}$, which is correct between 50% and 60% of the time depending upon the kinematics of the final state, is chosen in the q^2 and w determination as simulation studies have shown that this choice introduces the smallest bias. The w resolution is estimated from simulated data in different w intervals. The distributions of differences between reconstructed and generated w are fitted with double-Gaussian functions, and the effective standard deviations are found to be between 0.01 and 0.05. The overall w resolution is estimated with a fit with a triple-Gaussian function and has an effective standard deviation σ equal to 0.028.

IV. SPECTRAL DISTRIBUTION $dN_{\mathrm{corr}}/dw(\Lambda_b^0 \to \Lambda_c^+\mu^-\bar{\nu}_\mu)$

The $\Lambda_b^0 \to \Lambda_c^+\mu^-\bar{\nu}_\mu X$ candidates are separated into 14 equal-size bins of reconstructed w in the full kinematic range $1 \leq w \leq 1.43$. The parameters of the PDFs describing the signal and background components are determined from the fit to the overall $pK^-\pi^+$ mass spectrum. The contributions from semileptonic decays including higher-mass baryons in the final state is evaluated by fitting the $\Lambda_c^+\pi^+\pi^-$ mass spectra with two different methods. In the first, we fit for the four resonances shown in Fig. 2 using a PDF derived from the WS sample to model the background and then use the simulation to correct for efficiency. In the second, we determine the signal yields of the Λ_c^{*+} states by subtracting the WS background and treating the residual smooth component of the spectrum as originating from a semileptonic decay $\Lambda_b^0 \to \Lambda_c^+\mu^-\bar{\nu}_\mu X$. The second method provides an estimate of the systematic uncertainty introduced by the contribution from nonresonant $\Lambda_c^+\pi^+\pi^-$ components of the hadron spectrum, as the smooth component of this spectrum is likely to comprise also the combinatoric background.

Next, we correct the raw $\Lambda_c^+\mu^-\bar{\nu}_\mu X$ and $\Lambda_c^+\pi^+\pi^-\mu^-\bar{\nu}_\mu X$ signal yields for the corresponding software trigger efficiencies, which are derived with a data-driven method [30], based on the determination of $\Lambda_c^+\mu^-\bar{\nu}_\mu X$ events where a positive trigger decision is provided by the signal candidates and events where the trigger decision is independent of the signal. Then, we subtract the raw yields reported in Table II, scaled by the corresponding efficiency ratios $\frac{\varepsilon(\Lambda_b^0 \to \Lambda_c^+\mu^-\bar{\nu}_\mu X)}{\varepsilon(\Lambda_b^0 \to \Lambda_c^+\pi^+\pi^-\mu^-\bar{\nu}_\mu X)}$, from the corrected $\Lambda_c^+\mu^-\bar{\nu}_\mu X$ yields. These ratios are derived from $\Lambda_b^0 \to \Lambda_c(2595)^+\mu^-\bar{\nu}_\mu$ and $\Lambda_b^0 \to \Lambda_c(2625)^+\mu^-\bar{\nu}_\mu$ simulations. The higher-mass yields are scaled by an average of these two corrections, as no model for these semileptonic decays is available. These corrections account for the efficiency loss due to the reconstruction of the additional pion pairs, as well as for the unseen $\Lambda_b^0 \to \Lambda_c^+\pi^0\pi^0\mu^-\bar{\nu}_\mu X$ decay, and are only mildly dependent upon the invariant mass of the final state. The expectation is that $\Lambda_b^0 \to \Lambda_c^+\pi^+\pi^-\mu^-\bar{\nu}_\mu$ accounts for two-thirds of the inclusive dipion final state. We have checked this prediction by studying the inclusive final states $\Sigma_c^{++}\mu^-\bar{\nu}_\mu X$, $\Sigma_c^+\mu^-\bar{\nu}_\mu X$, and $\Sigma_c^0\mu^-\bar{\nu}_\mu X$. Taking into account the difference in the $\Lambda_c^+\pi^+\pi^-\mu^-\bar{\nu}_\mu X$ and $\Lambda_c^+\pi^0\mu^-\bar{\nu}_\mu X$ detection efficiencies, estimated with simulations, we measure the ratio $R = N(\Lambda_c^+\pi^+\pi^-)/N(\Lambda_c^+\pi^+\pi^- + \Lambda_c^+\pi^0\pi^0)$ with

$$R = \frac{N(\Sigma_c^{++}) + N(\Sigma_c^0)}{N(\Sigma_c^{++}) + N(\Sigma_c^0) + N(\Sigma_c^+) \cdot [\varepsilon(\Lambda_c^+\pi^+\pi^-\mu)/\varepsilon(\Lambda_c^+\pi^0\mu)]}, \tag{7}$$

where $N(\Sigma_c^{++})$ and $N(\Sigma_c^0)$ are the detected yields for the final states $\Sigma_c^{++}\pi^-\mu\nu$ and $\Sigma_c^0\pi^+\mu\nu$, $N(\Sigma_c^+)$ is the detected yield for
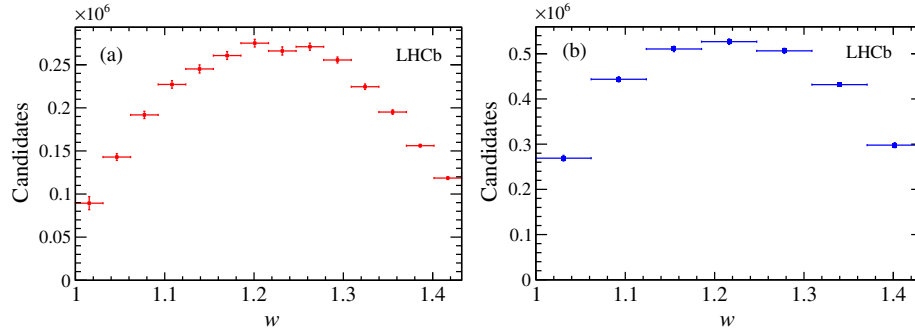
FIG. 3.   The spectra (a) dN_{meas}/dw before unfolding and (b) dN_{u}/dw after unfolding, for the decay $\Lambda_b^0 \to \Lambda_c^+ \mu^- \bar{\nu}_\mu$. The latter spectrum is then corrected for acceptance and reconstruction efficiency and fitted to the IW function $\xi_B(w)$ with the procedure discussed in the text.

the final state $\Sigma_c^+ \mu\nu X$, and $\varepsilon(\Lambda_c^+ \pi^+ \pi^- \mu)/\varepsilon(\Lambda_c^+ \pi^0 \mu)$ is the ratio between the reconstruction efficiencies of these final states calculated with simulation. A simulation study gives $\varepsilon(\Lambda_c^+ \pi^+ \pi^- \mu)/\varepsilon(\Lambda_c^+ \pi^0 \mu) = 25.9 \pm 2.7$, where the uncertainty reflects the limited sample size of the simulation. We obtain $R = 0.63 \pm 0.14$, where the statistical uncertainty is due to limited π^0 reconstruction efficiency, consistent with the expectation $R = 2/3$, and a negligible $\Sigma_c^+ \mu^- \bar{\nu}_\mu$ component in the denominator of Eq. (7).

The $\Lambda_b^0 \to \Lambda_c^+ \mu^- \bar{\nu}_\mu$ spectrum dN_{meas}/dw is then unfolded to account for the detector resolution and other w smearing effects such as the possible choice of the wrong solution of Eq. (6). The procedure adopted is based on the single value decomposition (SVD) method [41] using the RooUnfold package [42]. We choose to divide the unfolded spectrum dN_{u}/dw into seven w bins, to be consistent with the recommendation of Ref. [43] to divide the measured spectrum into a number of bins at least twice as many as the ones in the corrected spectrum. The SVD method includes a regularization procedure that depends upon a parameter k [41], ranging between unity and the number of degrees of freedom, in our case 14. Simulation studies demonstrate that $k = 4$ is optimal in our case. Variations associated with different choices of k have been studied and are included in the systematic

uncertainties. We have performed closure tests with different simulation models of the $\Lambda_b^0 \to \Lambda_c^+ \mu^- \bar{\nu}_\mu$ dynamics and verified that this unfolding procedure does not bias the reconstructed distribution. The spectra before and after unfolding are shown in Fig. 3. Finally, using simulated samples of signal events, we correct the unfolded spectrum for w-dependent acceptance and selection efficiency to obtain the distribution dN_{corr}/dw. Various kinematic distributions have been studied in simulation and data, and we find that they are all in good agreement.

V. SHAPE OF $\xi_B(w)$ FOR $\Lambda_b^0 \to \Lambda_c^+ \mu^- \bar{\nu}_\mu$ DECAYS

In order to determine the shape of the Isgur-Wise function $\xi_B(w)$, we use the square root of dN_{corr}/dw divided by the kinematic factor $K(\langle w \rangle)$, defined in Eq. (4), evaluated at the midpoint in the seven unfolded w bins. We derive the IW shape with a χ^2 fit, where the χ^2 is formed using the full covariance matrix of dN_{corr}/dw.

We use various functional forms to extract the slope, ρ^2, and curvature, σ^2, of $\xi_B(w)$. The first functional form is motivated by the $1/N_c$ expansion [44], where N_c represents the number of colors, and has an exponential shape parametrized as
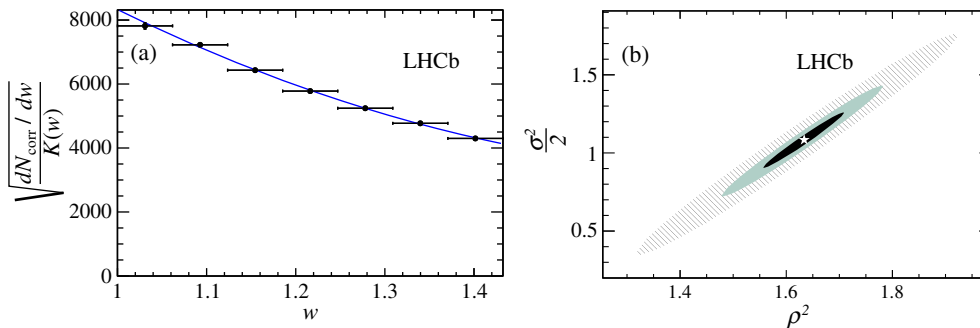

FIG. 4.   (a) The Isgur-Wise function fit for the decay $\Lambda_b^0 \to \Lambda_c^+ \mu^- \nu$ with a Taylor series expansion in $(w-1)$ up to second order. The black dots show the data, and the solid (blue) line shows the fitted function with the second-order Taylor series expansion model. The vertical scale is in arbitrary units. (b) The correlation between slope ρ^2 and curvature $\sigma^2/2$; the three ellipses correspond to the 1σ, 2σ, and 4σ contours.

TABLE III. Summary of the values for the slope and curvature of the Isgur-Wise function with different parametrizations. The quoted uncertainties are statistical only. The models marked with "*" have only the slope at zero recoil as a free parameter; thus, the curvature is derived from the fitted ρ^2.

Shape	ρ^2	σ^2	Correlation coefficient	χ^2/DOF
Exponential*	1.65 ± 0.03	2.72 ± 0.10	100%	5.3/5
Dipole*	1.82 ± 0.03	4.22 ± 0.12	100%	5.3/5
Taylor series	1.63 ± 0.07	2.16 ± 0.34	97%	4.5/4

$$\xi_B(w) = \exp[-\rho^2(w-1)]. \tag{8}$$

The second functional form, the so-called dipole IW function, which is more consistent with sum-rule bounds [17], is given by

$$\xi_B(w) = \left(\frac{2}{w+1}\right)^{2\rho^2}. \tag{9}$$

Finally, we can use a simple Taylor series expansion of the Isgur-Wise function and fit for the slope and curvature parameters using the Taylor series expansion introduced in Eq. (5). Figure 4 shows the measured $\xi_B(w)$ and the fit results with this parametrization. Table III summarizes the slope and curvature at zero recoil obtained with the three fit models. Note that the curvature is an independent parameter only in the last fit, while in the first two models, it is related to the second derivative of the IW function.

As the slope of the IW function is the most relevant quantity to determine $|V_{cb}|$ in the framework of HQET [13], we focus our studies on the systematic uncertainties on this parameter. We consider several sources of systematic uncertainties, which are listed in Table IV. The first two are determined by changing the fit models for Λ_c^+ and $\Lambda_c(2595)^+$ and $\Lambda_c(2625)^+$ signal shapes in the corresponding candidate mass spectra. The software trigger efficiency uncertainty is estimated by using an alternative procedure to evaluate this efficiency using the trigger emulation in the LHCb simulation. In order to assess systematics associated with the bin size, we perform the

TABLE IV. Summary of the systematic uncertainties on the slope parameter ρ^2. The total uncertainty is obtained by adding the individual components in quadrature.

Source	$\sigma(\rho^2)$
Signal fit for Λ_c^+	0.02
Signal PDF for Λ_c^{*+}	0.02
Software trigger efficiency	0.02
w binning	0.03
SVD unfolding regularization	0.03
Phase space averaging	0.03
$\Lambda_b^0 \to \Lambda_c^+ \mu^- \bar{\nu}_\mu$ modeling	0.03
$\Lambda_b^0 \to \Lambda_c^{*+} \mu^- \bar{\nu}_\mu$ modeling	0.03
Additional components of the semileptonic spectrum	0.02
Λ_b^0 kinematic dependencies	0.02
Total	0.08

analysis with different binning choices. The sensitivity to the $\Lambda_b^0 \to \Lambda_c^+ \mu^- \bar{\nu}_\mu$ form-factor modeling is assessed by reweighting the simulated w spectra to correspond to different ξ_B functions with slopes ranging from 1.5 to 1.7. The "phase space averaging" sensitivity is estimated by comparing the fit to the expression for dN_{corr}/dw with the fit to $1/K(\langle w \rangle)\sqrt{dN_{\text{corr}}/dw}$. The uncertainty associated with the $\Lambda_b^0 \to \Lambda_c^{*+} \mu^- \bar{\nu}_\mu$ modeling is evaluated by changing the relative fraction of $\Lambda_c^+ \pi^+ \pi^-$ versus $\Lambda_c^+ \pi^0 \pi^0$ of the Λ_c^{*+} spectrum by $\pm 20\%$. Finally, we use the alternative evaluation of the fraction of $\Lambda_b^0 \to \Lambda_c^+ \pi^+ \pi^- \mu^- \bar{\nu}_\mu$ which includes the maximum possible nonresonant component to assess the sensitivity to residual Λ_c^{*+} components in the subtracted spectrum. The total systematic uncertainty in ρ^2 is 0.08.

The value of ρ^2 obtained from the Taylor series expansion is

$$\rho^2 = 1.63 \pm 0.07 \pm 0.08,$$

which is consistent with lattice calculations [23], QCD sum rules [22], and relativistic quark model [21] expectations. The measured slope is compatible with theoretical predictions and with the bound $\rho^2 \geq 3/4$ [16]. The measured curvature σ^2 is compatible within uncertainties with the lower bound $\sigma^2 \geq 3/5[\rho^2 + (\rho^2)^2]$ [18].

VI. COMPARISON WITH UNQUENCHED LATTICE PREDICTIONS

The lattice QCD calculation in Ref. [19] uses a helicity-based description of the six form factors governing $\Lambda_b^0 \to \Lambda$ transitions introduced in Ref. [45]. The calculation uses state-of-the-art techniques encompassing the entire q^2 region. The stated uncertainties on the predicted width are therefore larger than what is expected in a high-q^2 region but remain rather small, namely 6.3%. This corresponds to a 3.2% theoretical uncertainty on $|V_{cb}|$, thus raising the prospect of an additional precise independent determination of $|V_{cb}|$.

The simplest check on this theoretical prediction consists of a comparison of the predicted shape of $d\Gamma/dq^2$ and the measured data. Thus, we measure the distribution dN_{corr}/dq^2 with the same procedure adopted to derive dN_{corr}/dw, including efficiency corrections and the unfolding procedure, with the same number of bins used to determine the raw and unfolded yields. We produce

seven corrected yields and their associated covariance matrix, where the nondiagonal terms are related to the unfolding procedure. We then perform a χ^2 fit to the seven experimental dN_{corr}/dq^2 data points using the theoretical functional shape given in Eq. (85) of Ref. [19], which also provides the nominal values of the form-factor parameters, and thus we leave only the relative normalization floating. This fit uses a covariance matrix that combines experimental and theoretical uncertainties, which yields a χ^2 equal to 1.32 for 6 degrees of freedom and a corresponding p-value of 97%. This shows that the predicted shape is in good agreement with our measurement.

The form-factor decomposition in Ref. [19] does not allow a straightforward extrapolation to the HQET limit of infinite heavy-quark masses. However, we know that in the static limit all the form factors are proportional to a single universal function. In order to assess how well our data are consistent with the static limit, we perform a second χ^2 fit assuming that all the form factors are proportional to a single z-expansion function [46]. Fits with different pole masses used in the six form factors determined in Ref. [19] are performed. The overall shape does not change appreciably; the pole mass of 6.768 GeV is preferred. The two fit parameters are the coefficients a_0 and a_1, giving the strength of the first two terms in the z-expansion. The resulting fitted shape is shown in Fig. 5. This fit has a χ^2 equal to 1.85 for 5 degrees of freedom, with a corresponding p-value of 87%. Note that the shape obtained with a single form factor is very similar to the one predicted in Ref. [19]. This is consistent with the HQET prediction [15] that the shape of the differential distribution is well described by the static approximation, modulo a scale correction of the order of 10%, reflecting higher-order contributions. Further details of this fit and the fit using the lattice QCD calculation can be found in the Appendix.
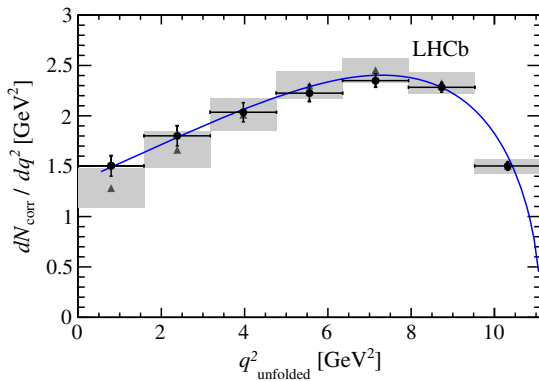

FIG. 5. Comparison between the fit to the seven experimental data points using either the lattice QCD calculation of Ref. [19], shown as gray points with a shaded area corresponding to the binned 1σ theory uncertainty, or a single form-factor fit in the z-expansion, shown as the solid blue curve. The data points, modulo a scale factor, are shown as black points with error bars.

VII. CONCLUSIONS

A precise measurement of the shape of the Isgur-Wise function describing the semileptonic decay $\Lambda_b^0 \to \Lambda_c^+ \mu^- \bar{\nu}_\mu$ has been performed. The measured slope is consistent with theoretical models and the bound $\rho^2 \geq 3/4$ [16]. The measured curvature σ^2 is consistent with the lower-bound constraint $\sigma^2 \geq 3/5[\rho^2 + (\rho^2)^2]$ [18]. The shape of $d\Gamma/dq^2$ is studied and found to be well described by the unquenched lattice QCD prediction of Ref. [19], as well as by a single form-factor parametrization. Further studies with a suitable normalization channel will lead to a precise independent determination of the CKM parameter $|V_{cb}|$.

ACKNOWLEDGMENTS

APPENDIX A: ANALYTICAL EXPRESSION FOR $d\Gamma/dq^2$

This Appendix describes the formalism used in the $d\Gamma/dq^2$ fits. In particular, we give the expression of $d\Gamma/dq^2$ in terms of the form-factor basis chosen in Ref. [19], the so-called helicity form factors. In addition, we show the corresponding expression used to model the static limit.

The lattice QCD calculations reported in Ref. [19] predict the differential decay width $d\Gamma(\Lambda_b^0 \to \Lambda_c^+ \mu^- \bar{\nu}_\mu)/dq^2$ as follows,

$$\frac{d\Gamma}{dq^2} = \frac{G_F^2|V_{cb}|^2\sqrt{s_+s_-}}{768\pi^3 m_{\Lambda_b^0}^3}\left(1-\frac{m_\ell^2}{q^2}\right)^2$$

$$\times\left\{4(m_\ell^2+2q^2)(s_+[g_\perp(q^2)]^2+s_-[f_\perp(q^2)]^2)\right.$$

$$+2\frac{m_\ell^2+2q^2}{q^2}(s_+[(m_{\Lambda_b^0}-m_X)g_+(q^2)]^2+s_-[(m_{\Lambda_b^0}+m_X)f_+(q^2)]^2)$$

$$\left.+\frac{6m_\ell^2}{q^2}(s_+[(m_{\Lambda_b^0}-m_X)f_0(q^2)]^2+s_-[(m_{\Lambda_b^0}+m_X)g_0(q^2)]^2)\right\},\tag{A1}$$

where $g_\perp$, $f_\perp$, g_+, f_+, g_0, and f_0 represent the six form factors necessary to describe this decay, $X\equiv\Lambda_c$ denotes the final-state baryon, m_ℓ represents the mass of the muon, q^2 is the squared four-momentum transfer between the heavy baryons, and

$$s_\pm=(m_{\Lambda_b^0}\pm m_X)^2-q^2.\tag{A2}$$

The six form factors are cast in terms of the z-expansion [46] up to first order and have the functional form

$$f(q^2)=\frac{1}{1-q^2/(m_{\text{pole}}^f)^2}$$
$$\times[a_0^f+a_1^f z^f(q^2)],\tag{A3}$$

where $z^f(q^2)$ is given by

$$z^f(q^2)=\frac{\sqrt{t_+^f-q^2}-\sqrt{t_+^f-t_0}}{\sqrt{t_+^f-q^2}+\sqrt{t_+^f-t_0}},\tag{A4}$$

$$t_0=(m_{\Lambda_b^0}-m_X)^2,\tag{A5}$$

and t_+^f is given by

$$t_+^f=(m_{\text{pole}}^f)^2,\tag{A6}$$

and the pole masses used in the calculations are shown in Table V. The parameters a_0^f and a_1^f for the six form factors describing this decay are given in Table VIII of Ref. [19].

In the static limit, all the helicity form factors are proportional to a single universal function. Thus, we use a common z-expansion parametrization

$$\frac{d\Gamma}{dq^2}=\frac{G_F^2|V_{cb}|^2\sqrt{s_+s_-}}{768\pi^3 m_{\Lambda_b^0}^3}\left(1-\frac{m_\ell^2}{q^2}\right)^2 g_\perp^2(q^2)$$

$$\times\left\{4(m_\ell^2+2q^2)(s_++s_-)\right.$$

$$\left.+\frac{4}{q^2}[s_+(m_{\Lambda_b^0}-m_X)^2+s_-(m_{\Lambda_b^0}+m_X)^2][2m_\ell^2+q^2]\right\},\tag{A7}$$

where the choice of $g_\perp$ reflects the choice of the pole mass used in the single z-expansion fit given in Sec. VI. We performed the fits with various choices of pole masses and examined the effects on the shape $d\Gamma/dq^2$ and found the shape did not vary significantly, though it was found that the parameters defining $g_\perp$ yielded the optimal fit. In this case, the fit parameters are the coefficients a_0 and a_1 in the z-expansion parametrization of $g_\perp(q^2)$, which has the form shown in Eq. (A3).

APPENDIX B: MEASURED NORMALIZED SPECTRA dN_{corr}/dq^2 AND ASSOCIATED COVARIANCE MATRIX

In this Appendix, we report the seven measured data points dN_{corr}/dq^2 and the corresponding covariance matrix, shown in Tables VI and VII, respectively.

TABLE V. Masses of the relevant form-factor poles in the physical limit (in GeV).

f	J^P	$m_{\text{pole}}^f(\Lambda_b^0\to\Lambda_c)$ (GeV)
f_+, $f_\perp$	1^-	6.332
f_0	0^+	6.725
g_+, $g_\perp$	1^+	6.768
g_0	0^-	6.276

TABLE VI. Measured normalized yields $dN_{\text{corr}}(\Lambda_b^0\to\Lambda_c^+\mu^-\bar{\nu}_\mu)/dq^2$.

q^2 (GeV^2)	dN_{corr}/dq^2
0.80	1.50 ± 0.10
2.38	1.80 ± 0.10
3.97	2.04 ± 0.10
5.56	2.23 ± 0.08
7.14	2.35 ± 0.07
8.73	2.28 ± 0.05
10.32	1.50 ± 0.04

TABLE VII.   Covariance matrix of the measured normalized yields $\mathrm{Cov}[dN_{\mathrm{corr}}(\Lambda_b^0 \to \Lambda_c^+ \mu^- \bar{\nu}_\mu)/dq^2]$.

q^2 (GeV^2)	dN_{corr}/dq^2						
0.80	0.0103	0.0052	−0.0032	−0.0033	−0.0009	0.0004	0.0005
2.38	0.0052	0.0100	0.0044	0.0011	−0.0002	−0.0006	0.0002
3.97	−0.0032	0.0044	0.0090	0.0048	0.0004	−0.0013	−0.0007
5.56	−0.0035	−0.0011	0.0048	0.0070	0.0031	−0.0006	−0.0013
7.14	−0.0009	−0.0019	−0.0004	0.0031	0.0044	0.0015	0.0006
8.73	0.0004	−0.0006	−0.0013	−0.0006	0.0015	0.0023	0.0013
10.32	0.0005	0.0002	−0.0007	−0.0013	−0.0006	0.0013	0.0018

[1] J. L. Rosner, The CKM matrix and *B* physics, J. Phys. G **18,** 1575 (1992).

[2] J. Charles *et al.* (CKM Fitter Group Collaboration), Current status of the Standard Model CKM fit and constraints on $\Delta F = 2$ new physics, Phys. Rev. D **91,** 073007 (2015), updated results and plots available at http://ckmfitter.in2p3 .fr/.

[3] M. Bona *et al.* (UTfit Collaboration), Latest results for the unitary triangle fit from the UTfit collaboration, *Proc. Sci.*, CKM2016 (2017) 96.

[4] D. Fakirov and B. Stech, F- and D-decays, Nucl. Phys. **B133,** 315 (1978).

[5] M. Bauer, B. Stech, and M. Wirbel, Exclusive nonleptonic decays of D, D_s, and B mesons, Z. Phys. C **34,** 103 (1987).

[6] N. Isgur and M. B. Wise, Weak decays of heavy mesons in the static quark approximation, Phys. Lett. B **232,** 113 (1989).

[7] C. T. Sachrajda, Lattice quantum chromodynamics, Adv. Ser. Dir. High Energy Phys. **26,** 93 (2016).

[8] T. Mannel and D. van Dyk, Zero-recoil sum rules for $\Lambda_b \to \Lambda_c$ form factors, Phys. Lett. B **751,** 48 (2015).

[9] N. Isgur and M. B. Wise, Heavy baryon weak form factors, Nucl. Phys. **B348,** 276 (1991).

[10] I. I. Bigi, T. Mannel, and N. Uraltsev, Semileptonic width ratios among beauty hadrons, J. High Energy Phys. 09 (2011) 012.

[11] A. F. Falk and M. Neubert, Second order power corrections in the heavy-quark effective theory. I. Formalism and meson form factors, Phys. Rev. D **47,** 2965 (1993).

[12] H. Georgi, B. Grinstein, and M. B. Wise, Λ_b semileptonic decay form factors for $m_c \neq \infty$, Phys. Lett. B **252,** 456 (1990).

[13] A. F. Falk and M. Neubert, Second order power corrections in the heavy-quark effective theory. II Baryon form factors, Phys. Rev. D **47,** 2982 (1993).

[14] C. Patrignani *et al.* (Particle Data Group Collaboration), Review of particle physics, Chin. Phys. C **40,** 100001 (2016).

[15] B. Holdom, M. Sutherland, and J. Mureika, Comparison of $1/m_Q^2$ corrections in mesons and baryons, Phys. Rev. D **49,** 2359 (1994).

[16] A. Le Yaouanc, L. Oliver, and J. C. Raynal, Lower bounds on the curvature of the Isgur-Wise function, Phys. Rev. D **69,** 094022 (2004).

[17] A. Le Yaouanc, L. Oliver, and J. C. Raynal, Isgur-Wise functions and unitary representations of the Lorentz group: The baryon case $j = 0$, Phys. Rev. D **80,** 054006 (2009).

[18] A. Le Yaouanc, L. Oliver, and J. C. Raynal, Bound on the curvature of the Isgur-Wise function of the baryon semileptonic decay $\Lambda_b \to \Lambda_c \ell \bar{\nu}_\ell$, Phys. Rev. D **79,** 014023 (2009).

[19] W. Detmold, C. Lehner, and S. Meinel, $\Lambda_b \to p \ell^- \bar{\nu}_\ell$ and $\Lambda_b \to \Lambda_c \ell^- \bar{\nu}_\ell$ form factors from lattice QCD with relativistic heavy quarks, Phys. Rev. D **92,** 034503 (2015).

[20] J. Abdallah *et al.* (DELPHI Collaboration), Measurement of the Λ_b^0 decay form factor, Phys. Lett. B **585,** 63 (2004).

[21] D. Ebert, R. N. Faustov, and V. O. Galkin, Semileptonic decays of heavy baryons in the relativistic quark model, Phys. Rev. D **73,** 094002 (2006).

[22] M.-Q. Huang, H.-Y. Jin, J. G. Korner, and C. Liu, Note on the slope parameter of the baryonic $\Lambda_b \to \Lambda_c$ Isgur-Wise function, Phys. Lett. B **629,** 27 (2005).

[23] K. C. Bowler, R. D. Kenway, L. Lellouch, J. Nieves, O. Oliveira, D. G. Richards, C. T. Sachrajda, N. Stella, and P. Ueberholz (UKQCD Collaboration), First lattice study of semileptonic decays of Λ_b and Ξ_b baryons, Phys. Rev. D **57,** 6948 (1998).

[24] A. A. Alves, Jr. *et al.* (LHCb Collaboration), The LHCb Detector at the LHC, J. Instrum. **3,** S08005 (2008).

[25] R. Aaij *et al.* (LHCb Collaboration), LHCb detector performance, Int. J. Mod. Phys. A **A30,** 1530022 (2015).

[26] R. Aaij *et al.*, Performance of the LHCb Vertex Locator, J. Instrum. **9,** P09007 (2014).

[27] R. Arink *et al.*, Performance of the LHCb Outer Tracker, J. Instrum. **9,** P01002 (2014).

[28] M. Adinolfi *et al.*, Performance of the LHCb RICH detector at the LHC, Eur. Phys. J. C **73,** 2431 (2013).

[29] A. A. Alves Jr. *et al.*, Performance of the LHCb muon system, J. Instrum. **8,** P02022 (2013).

[30] R. Aaij *et al.*, The LHCb trigger and its performance in 2011, J. Instrum. **8,** P04022 (2013).

[31] T. Sjöstrand, S. Mrenna, and P. Skands, PYTHIA 6.4 physics and manual, J. High Energy Phys. 05 (2006) 026; T. Sjöstrand, S. Mrenna, and P. Skands, A brief introduction to PYTHIA 8.1, Comput. Phys. Commun. **178,** 852 (2008).

[32] I. Belyaev et al., Handling of the generation of primary events in Gauss, the LHCb simulation framework, J. Phys. Conf. Ser. **331,** 032047 (2011).

[33] D. J. Lange, The EvtGen particle decay simulation package, Nucl. Instrum. Methods Phys. Res., Sect. A **462,** 152 (2001).

[34] P. Golonka and Z. Was, PHOTOS Monte Carlo: A precision tool for QED corrections in Z and W decays, Eur. Phys. J. C **45,** 97 (2006).

[35] J. Allison et al. (GEANT4 Collaboration), Geant4 developments and applications, IEEE Trans. Nucl. Sci. **53,** 270 (2006); S. Agostinelli et al. (GEANT4 Collaboration), Geant4: A simulation toolkit, Nucl. Instrum. Methods Phys. Res., Sect. A **506,** 250 (2003).

[36] M. Clemencic, G. Corti, S. Easo, C. R. Jones, S. Miglioranzi, M. Pappagallo, and P. Robbe, The LHCb simulation application, Gauss: Design, evolution and experience, J. Phys. Conf. Ser. **331,** 032023 (2011).

[37] R. Aaij et al. (LHCb Collaboration), Measurement of $\sigma(pp \to b\bar{b}X)$ at $\sqrt{s} = 7$ TeV in the forward region, Phys. Lett. B **694,** 209 (2010).

[38] C. Albertus, E. Hernandez, and J. Nieves, Nonrelativistic constituent quark model and HQET combined study of semileptonic decays of Λ_b and Ξ_b baryons, Phys. Rev. D **71,** 014012 (2005).

[39] M. Pervin, W. Roberts, and S. Capstick, Semileptonic decays of heavy Λ baryons in a quark model, Phys. Rev. C **72,** 035201 (2005).

[40] A. K. Leibovich and I. W. Stewart, Semileptonic Λ_b decay to excited Λ_c baryons at order Λ_{QCD}/m_Q, Phys. Rev. D **57,** 5620 (1998).

[41] A. Hoecker and V. Kartvelishvili, SVD approach to data unfolding, Nucl. Instrum. Methods Phys. Res., Sect. A **372,** 469 (1996).

[42] T. Adye, Unfolding algorithms and tests using RooUnfold, in Proceedings, PHYSTAT 2011 Workshop on Statistical Issues Related to Discovery Claims in Search Experiments and Unfolding, CERN, Geneva, Switzerland, 2011 (CERN, Geneva, 2011), p. 313, https://cds.cern.ch/record/1349242?ln=en.

[43] V. Blobel, in Terascale Statistics Tools School Spring 2010, LOCATION, 2010 (unpublished).

[44] E. E. Jenkins, A. V. Manohar, and M. B. Wise, The baryon Isgur-Wise function in the large N_c limit, Nucl. Phys. **B396,** 38 (1993).

[45] T. Feldmann and M. W. Y. Yip, Form factors for $\Lambda_b \to \Lambda$ transitions in SCET, Phys. Rev. D **85,** 014035 (2012); Erratum, Phys. Rev. D **86,** 079901 (2012).

[46] R. J. Hill, The Modern description of semileptonic meson form factors, Proceedings, 4th Conference on Flavor Physics and CP Violation (FPCP 2006): Vancouver, British Columbia, Canada, eConf C060409, 027 (2006).

R. Aaij,[40] B. Adeva,[39] M. Adinolfi,[48] Z. Ajaltouni,[5] S. Akar,[59] J. Albrecht,[10] F. Alessio,[40] M. Alexander,[53] A. Alfonso Albero,[38] S. Ali,[43] G. Alkhazov,[31] P. Alvarez Cartelle,[55] A. A. Alves Jr.,[59] S. Amato,[2] S. Amerio,[23] Y. Amhis,[7] L. An,[3] L. Anderlini,[18] G. Andreassi,[41] M. Andreotti,[17,g] J. E. Andrews,[60] R. B. Appleby,[56] F. Archilli,[43] P. d'Argent,[12] J. Arnau Romeu,[6] A. Artamonov,[37] M. Artuso,[61] E. Aslanides,[6] G. Auriemma,[26] M. Baalouch,[5] I. Babuschkin,[56] S. Bachmann,[12] J. J. Back,[50] A. Badalov,[38] C. Baesso,[62] S. Baker,[55] V. Balagura,[7,c] W. Baldini,[17] A. Baranov,[35] R. J. Barlow,[56] C. Barschel,[40] S. Barsuk,[7] W. Barter,[56] F. Baryshnikov,[32] M. Baszczyk,[27,l] V. Batozskaya,[29] V. Battista,[41] A. Bay,[41] L. Beaucourt,[4] J. Beddow,[53] F. Bedeschi,[24] I. Bediaga,[1] A. Beiter,[61] L. J. Bel,[43] N. Beliy,[63] V. Bellee,[41] N. Belloli,[21,i] K. Belous,[37] I. Belyaev,[32] E. Ben-Haim,[8] G. Bencivenni,[19] S. Benson,[43] S. Beranek,[9] A. Berezhnoy,[33] R. Bernet,[42] D. Berninghoff,[12] E. Bertholet,[8] A. Bertolin,[23] C. Betancourt,[42] F. Betti,[15] M.-O. Bettler,[40] M. van Beuzekom,[43] Ia. Bezshyiko,[42] S. Bifani,[47] P. Billoir,[8] A. Birnkraut,[10] A. Bitadze,[56] A. Bizzeti,[18,u] M. B. Bjoern,[57] T. Blake,[50] F. Blanc,[41] J. Blouw,[11,†] S. Blusk,[61] V. Bocci,[26] T. Boettcher,[58] A. Bondar,[36,w] N. Bondar,[31] W. Bonivento,[16] I. Bordyuzhin,[32] A. Borgheresi,[21,i] S. Borghi,[56] M. Borisyak,[35] M. Borsato,[39] M. Borysova,[46] F. Bossu,[7] S. Boubdir,[9] T. J. V. Bowcock,[54] E. Bowen,[42] C. Bozzi,[17,40] S. Braun,[12] T. Britton,[61] J. Brodzicka,[56] D. Brundu,[16] E. Buchanan,[48] C. Burr,[56] A. Bursche,[16,f] J. Buytaert,[40] W. Byczynski,[40] S. Cadeddu,[16] H. Cai,[64] R. Calabrese,[17,g] R. Calladine,[47] M. Calvi,[21,i] M. Calvo Gomez,[38,m] A. Camboni,[38] P. Campana,[19] D. H. Campora Perez,[40] L. Capriotti,[56] A. Carbone,[15,e] G. Carboni,[25,j] R. Cardinale,[20,h] A. Cardini,[16] P. Carniti,[21,i] L. Carson,[52] K. Carvalho Akiba,[2] G. Casse,[54] L. Cassina,[21,i] L. Castillo Garcia,[41] M. Cattaneo,[40] G. Cavallero,[20,40,h] R. Cenci,[24,t] D. Chamont,[7] M. Charles,[8] Ph. Charpentier,[40] G. Chatzikonstantinidis,[47] M. Chefdeville,[4] S. Chen,[56] S. F. Cheung,[57] S.-G. Chitic,[40] V. Chobanova,[39] M. Chrzaszcz,[42,27] A. Chubykin,[31] X. Cid Vidal,[39] G. Ciezarek,[43] P. E. L. Clarke,[52] M. Clemencic,[40] H. V. Cliff,[49] J. Closier,[40] V. Coco,[59] J. Cogan,[6] E. Cogneras,[5] V. Cogoni,[16,f] L. Cojocariu,[30] P. Collins,[40] T. Colombo,[40] A. Comerma-Montells,[12] A. Contu,[40] A. Cook,[48] G. Coombs,[40] S. Coquereau,[38] G. Corti,[40] M. Corvo,[17,g] C. M. Costa Sobral,[50] B. Couturier,[40] G. A. Cowan,[52] D. C. Craik,[52] A. Crocombe,[50] M. Cruz Torres,[62] R. Currie,[52] C. D'Ambrosio,[40] F. Da Cunha Marinho,[2] E. Dall'Occo,[43] J. Dalseno,[48] A. Davis,[3] O. De Aguiar Francisco,[54] K. De Bruyn,[6] S. De Capua,[56] M. De Cian,[12] J. M. De Miranda,[1] L. De Paula,[2] M. De Serio,[14,d]

P. De Simone,[19] C. T. Dean,[53] D. Decamp,[4] L. Del Buono,[8] H.-P. Dembinski,[11] M. Demmer,[10] A. Dendek,[28] D. Derkach,[35] O. Deschamps,[5] F. Dettori,[54] B. Dey,[65] A. Di Canto,[40] P. Di Nezza,[19] H. Dijkstra,[40] F. Dordei,[40] M. Dorigo,[41] A. Dosil Suárez,[39] L. Douglas,[53] A. Dovbnya,[45] K. Dreimanis,[54] L. Dufour,[43] G. Dujany,[8] K. Dungs,[40] P. Durante,[40] R. Dzhelyadin,[37] M. Dziewiecki,[12] A. Dziurda,[40] A. Dzyuba,[31] N. Déléage,[4] S. Easo,[51] M. Ebert,[52] U. Egede,[55] V. Egorychev,[32] S. Eidelman,[36,w] S. Eisenhardt,[52] U. Eitschberger,[10] R. Ekelhof,[10] L. Eklund,[53] S. Ely,[61] S. Esen,[12] H. M. Evans,[49] T. Evans,[57] A. Falabella,[15] N. Farley,[47] S. Farry,[54] R. Fay,[54] D. Fazzini,[21,i] L. Federici,[25] D. Ferguson,[52] G. Fernandez,[38] P. Fernandez Declara,[40] A. Fernandez Prieto,[39] F. Ferrari,[15] F. Ferreira Rodrigues,[2] M. Ferro-Luzzi,[40] S. Filippov,[34] R. A. Fini,[14] M. Fiore,[17,g] M. Fiorini,[17,g] M. Firlej,[28] C. Fitzpatrick,[41] T. Fiutowski,[28] F. Fleuret,[7,b] K. Fohl,[40] M. Fontana,[16,40] F. Fontanelli,[20,h] D. C. Forshaw,[61] R. Forty,[40] V. Franco Lima,[54] M. Frank,[40] C. Frei,[40] J. Fu,[22,q] W. Funk,[40] E. Furfaro,[25,j] C. Färber,[40] E. Gabriel,[52] A. Gallas Torreira,[39] D. Galli,[15,e] S. Gallorini,[23] S. Gambetta,[52] M. Gandelman,[2] P. Gandini,[57] Y. Gao,[3] L. M. Garcia Martin,[70] J. García Pardiñas,[39] J. Garra Tico,[49] L. Garrido,[38] P. J. Garsed,[49] D. Gascon,[38] C. Gaspar,[40] L. Gavardi,[10] G. Gazzoni,[5] D. Gerick,[12] E. Gersabeck,[12] M. Gersabeck,[56] T. Gershon,[50] Ph. Ghez,[4] S. Gianì,[41] V. Gibson,[49] O. G. Girard,[41] L. Giubega,[30] K. Gizdov,[52] V. V. Gligorov,[8] D. Golubkov,[32] A. Golutvin,[55,40] A. Gomes,[1,a] I. V. Gorelov,[33] C. Gotti,[21,i] E. Govorkova,[43] J. P. Grabowski,[12] R. Graciani Diaz,[38] L. A. Granado Cardoso,[40] E. Graugés,[38] E. Graverini,[42] G. Graziani,[18] A. Grecu,[30] R. Greim,[9] P. Griffith,[16] L. Grillo,[21,40,i] L. Gruber,[40] B. R. Gruberg Cazon,[57] O. Grünberg,[67] E. Gushchin,[34] Yu. Guz,[37] T. Gys,[40] C. Göbel,[62] T. Hadavizadeh,[57] C. Hadjivasiliou,[5] G. Haefeli,[41] C. Haen,[40] S. C. Haines,[49] B. Hamilton,[60] X. Han,[12] T. Hancock,[57] S. Hansmann-Menzemer,[12] N. Harnew,[57] S. T. Harnew,[48] J. Harrison,[56] M. Hatch,[40] J. He,[63] M. Hecker,[55] A. Heister,[9] K. Hennessy,[54] P. Henrard,[5] L. Henry,[70] E. van Herwijnen,[40] M. Heß,[67] A. Hicheur,[2] D. Hill,[57] C. Hombach,[56] P. H. Hopchev,[41] Z.-C. Huard,[59] W. Hulsbergen,[43] T. Humair,[55] M. Hushchyn,[35] D. Hutchcroft,[54] M. Idzik,[28] P. Ilten,[58] R. Jacobsson,[40] J. Jalocha,[57] E. Jans,[43] A. Jawahery,[60] F. Jiang,[3] M. John,[57] D. Johnson,[40] C. R. Jones,[49] C. Joram,[40] B. Jost,[40] N. Jurik,[57] S. Kandybei,[45] M. Karacson,[40] J. M. Kariuki,[48] S. Karodia,[53] M. Kecke,[12] M. Kelsey,[61] M. Kenzie,[49] T. Ketel,[44] E. Khairullin,[35] B. Khanji,[12] C. Khurewathanakul,[41] T. Kirn,[9] S. Klaver,[56] K. Klimaszewski,[29] T. Klimkovich,[11] S. Koliiev,[46] M. Kolpin,[12] I. Komarov,[41] R. Kopecna,[12] P. Koppenburg,[43] A. Kosmyntseva,[32] S. Kotriakhova,[31] M. Kozeiha,[5] L. Kravchuk,[34] M. Kreps,[50] P. Krokovny,[36,w] F. Kruse,[10] W. Krzemien,[29] W. Kucewicz,[27,l] M. Kucharczyk,[27] V. Kudryavtsev,[36,w] A. K. Kuonen,[41] K. Kurek,[29] T. Kvaratskheliya,[32,40] D. Lacarrere,[40] G. Lafferty,[56] A. Lai,[16] G. Lanfranchi,[19] C. Langenbruch,[9] T. Latham,[50] C. Lazzeroni,[47] R. Le Gac,[6] J. van Leerdam,[43] A. Leflat,[33,40] J. Lefrançois,[7] R. Lefèvre,[5] F. Lemaitre,[40] E. Lemos Cid,[39] O. Leroy,[6] T. Lesiak,[27] B. Leverington,[12] T. Li,[3] Y. Li,[7] Z. Li,[61] T. Likhomanenko,[35,68] R. Lindner,[40] F. Lionetto,[42] X. Liu,[3] D. Loh,[50] I. Longstaff,[53] J. H. Lopes,[2] D. Lucchesi,[23,o] M. Lucio Martinez,[39] H. Luo,[52] A. Lupato,[23] E. Luppi,[17,g] O. Lupton,[40] A. Lusiani,[24] X. Lyu,[63] F. Machefert,[7] F. Maciuc,[30] V. Macko,[41] B. Maddock,[59] S. Maddrell-Mander,[48] O. Maev,[31] K. Maguire,[56] D. Maisuzenko,[31] M. W. Majewski,[28] S. Malde,[57] A. Malinin,[68] T. Maltsev,[36] G. Manca,[16,f] G. Mancinelli,[6] P. Manning,[61] D. Marangotto,[22,q] J. Maratas,[5,v] J. F. Marchand,[4] U. Marconi,[15] C. Marin Benito,[38] M. Marinangeli,[41] P. Marino,[24,t] J. Marks,[12] G. Martellotti,[26] M. Martin,[6] M. Martinelli,[41] D. Martinez Santos,[39] F. Martinez Vidal,[70] D. Martins Tostes,[2] L. M. Massacrier,[7] A. Massafferri,[1] R. Matev,[40] A. Mathad,[50] Z. Mathe,[40] C. Matteuzzi,[21] A. Mauri,[42] E. Maurice,[7,b] B. Maurin,[41] A. Mazurov,[47] M. McCann,[55,40] A. McNab,[56] R. McNulty,[13] J. V. Mead,[54] B. Meadows,[59] C. Meaux,[6] F. Meier,[10] N. Meinert,[67] D. Melnychuk,[29] M. Merk,[43] A. Merli,[22,40,q] E. Michielin,[23] D. A. Milanes,[66] E. Millard,[50] M.-N. Minard,[4] L. Minzoni,[17] D. S. Mitzel,[12] A. Mogini,[8] J. Molina Rodriguez,[1] I. A. Monroy,[66] S. Monteil,[5] M. Morandin,[23] M. J. Morello,[24,t] O. Morgunova,[68] J. Moron,[28] A. B. Morris,[52] R. Mountain,[61] F. Muheim,[52] M. Mulder,[43] M. Mussini,[15] D. Müller,[56] J. Müller,[10] K. Müller,[42] V. Müller,[10] P. Naik,[48] T. Nakada,[41] R. Nandakumar,[51] A. Nandi,[57] I. Nasteva,[2] M. Needham,[52] N. Neri,[22,40] S. Neubert,[12] N. Neufeld,[40] M. Neuner,[12] T. D. Nguyen,[41] C. Nguyen-Mau,[41,n] S. Nieswand,[9] R. Niet,[10] N. Nikitin,[33] T. Nikodem,[12] A. Nogay,[68] D. P. O'Hanlon,[50] A. Oblakowska-Mucha,[28] V. Obraztsov,[37] S. Ogilvy,[19] R. Oldeman,[16,f] C. J. G. Onderwater,[71] A. Ossowska,[27] J. M. Otalora Goicochea,[2] P. Owen,[42] A. Oyanguren,[70] P. R. Pais,[41] A. Palano,[14,d] M. Palutan,[19,40] A. Papanestis,[51] M. Pappagallo,[14,d] L. L. Pappalardo,[17,g] C. Pappenheimer,[59] W. Parker,[60] C. Parkes,[56] G. Passaleva,[18] A. Pastore,[14,d] M. Patel,[55] C. Patrignani,[15,e] A. Pearce,[40] A. Pellegrino,[43] G. Penso,[26] M. Pepe Altarelli,[40] S. Perazzini,[40] P. Perret,[5] L. Pescatore,[41] K. Petridis,[48] A. Petrolini,[20,h] A. Petrov,[68] M. Petruzzo,[22,q] E. Picatoste Olloqui,[38] B. Pietrzyk,[4] M. Pikies,[27] D. Pinci,[26] A. Pistone,[20,h] A. Piucci,[12] V. Placinta,[30] S. Playfer,[52] M. Plo Casasus,[39] T. Poikela,[40] F. Polci,[8] M. Poli Lener,[19] A. Poluektov,[50,36] I. Polyakov,[61] E. Polycarpo,[2] G. J. Pomery,[48] S. Ponce,[40] A. Popov,[37] D. Popov,[11,40] S. Poslavskii,[37] C. Potterat,[2] E. Price,[48] J. Prisciandaro,[39] C. Prouve,[48] V. Pugatch,[46] A. Puig Navarro,[42] H. Pullen,[57]

G. Punzi,[24,p] W. Qian,[50] R. Quagliani,[7,48] B. Quintana,[5] B. Rachwal,[28] J. H. Rademacker,[48] M. Rama,[24] M. Ramos Pernas,[39] M. S. Rangel,[2] I. Raniuk,[45,†] F. Ratnikov,[35] G. Raven,[44] M. Ravonel Salzgeber,[40] M. Reboud,[4] F. Redi,[55] S. Reichert,[10] A. C. dos Reis,[1] C. Remon Alepuz,[70] V. Renaudin,[7] S. Ricciardi,[51] S. Richards,[48] M. Rihl,[40] K. Rinnert,[54] V. Rives Molina,[38] P. Robbe,[7] A. B. Rodrigues,[1] E. Rodrigues,[59] J. A. Rodriguez Lopez,[66] P. Rodriguez Perez,[56,†] A. Rogozhnikov,[35] S. Roiser,[40] A. Rollings,[57] V. Romanovskiy,[37] A. Romero Vidal,[39] J. W. Ronayne,[13] M. Rotondo,[19] M. S. Rudolph,[61] T. Ruf,[40] P. Ruiz Valls,[70] J. Ruiz Vidal,[70] J. J. Saborido Silva,[39] E. Sadykhov,[32] N. Sagidova,[31] B. Saitta,[16,f] V. Salustino Guimaraes,[1] D. Sanchez Gonzalo,[38] C. Sanchez Mayordomo,[70] B. Sanmartin Sedes,[39] R. Santacesaria,[26] C. Santamarina Rios,[39] M. Santimaria,[19] E. Santovetti,[25,j] G. Sarpis,[56] A. Sarti,[26] C. Satriano,[26,s] A. Satta,[25] D. M. Saunders,[48] D. Savrina,[32,33] S. Schael,[9] M. Schellenberg,[10] M. Schiller,[53] H. Schindler,[40] M. Schlupp,[10] M. Schmelling,[11] T. Schmelzer,[10] B. Schmidt,[40] O. Schneider,[41] A. Schopper,[40] H. F. Schreiner,[59] K. Schubert,[10] M. Schubiger,[41] M.-H. Schune,[7] R. Schwemmer,[40] B. Sciascia,[19] A. Sciubba,[26,k] A. Semennikov,[32] A. Sergi,[47] N. Serra,[42] J. Serrano,[6] L. Sestini,[23] P. Seyfert,[40] M. Shapkin,[37] I. Shapoval,[45] Y. Shcheglov,[31] T. Shears,[54] L. Shekhtman,[36,w] V. Shevchenko,[68] B. G. Siddi,[17,40] R. Silva Coutinho,[42] L. Silva de Oliveira,[2] G. Simi,[23,o] S. Simone,[14,d] M. Sirendi,[49] N. Skidmore,[48] T. Skwarnicki,[61] E. Smith,[55] I. T. Smith,[52] J. Smith,[49] M. Smith,[55] l. Soares Lavra,[1] M. D. Sokoloff,[59] F. J. P. Soler,[53] B. Souza De Paula,[2] B. Spaan,[10] P. Spradlin,[53] S. Sridharan,[40] F. Stagni,[40] M. Stahl,[12] S. Stahl,[40] P. Stefko,[41] S. Stefkova,[55] O. Steinkamp,[42] S. Stemmle,[12] O. Stenyakin,[37] H. Stevens,[10] S. Stone,[61] B. Storaci,[42] S. Stracka,[24,p] M. E. Stramaglia,[41] M. Straticiuc,[30] U. Straumann,[42] L. Sun,[64] W. Sutcliffe,[55] K. Swientek,[28] V. Syropoulos,[44] M. Szczekowski,[29] T. Szumlak,[28] M. Szymanski,[63] S. T'Jampens,[4] A. Tayduganov,[6] T. Tekampe,[10] G. Tellarini,[17,g] F. Teubert,[40] E. Thomas,[40] J. van Tilburg,[43] M. J. Tilley,[55] V. Tisserand,[4] M. Tobin,[41] S. Tolk,[49] L. Tomassetti,[17,g] D. Tonelli,[24] S. Topp-Joergensen,[57] F. Toriello,[61] R. Tourinho Jadallah Aoude,[1] E. Tournefier,[4] M. Traill,[53] M. T. Tran,[41] M. Tresch,[42] A. Trisovic,[40] A. Tsaregorodtsev,[6] P. Tsopelas,[43] A. Tully,[49] N. Tuning,[43] A. Ukleja,[29] A. Ustyuzhanin,[35] U. Uwer,[12] C. Vacca,[16,f] A. Vagner,[69] V. Vagnoni,[15,40] A. Valassi,[40] S. Valat,[40] G. Valenti,[15] R. Vazquez Gomez,[19] P. Vazquez Regueiro,[39] S. Vecchi,[17] M. van Veghel,[43] J. J. Velthuis,[48] M. Veltri,[18,r] G. Veneziano,[57] A. Venkateswaran,[61] T. A. Verlage,[9] M. Vernet,[5] M. Vesterinen,[57] J. V. Viana Barbosa,[40] B. Viaud,[7] D. Vieira,[63] M. Vieites Diaz,[39] H. Viemann,[67] X. Vilasis-Cardona,[38,m] M. Vitti,[49] V. Volkov,[33] A. Vollhardt,[42] B. Voneki,[40] A. Vorobyev,[31] V. Vorobyev,[36,w] C. Voß,[9] J. A. de Vries,[43] C. Vázquez Sierra,[39] R. Waldi,[67] C. Wallace,[50] R. Wallace,[13] J. Walsh,[24] J. Wang,[61] D. R. Ward,[49] H. M. Wark,[54] N. K. Watson,[47] D. Websdale,[55] A. Weiden,[42] M. Whitehead,[40] J. Wicht,[50] G. Wilkinson,[57,40] M. Wilkinson,[61] M. Williams,[56] M. P. Williams,[47] M. Williams,[58] T. Williams,[47] F. F. Wilson,[51] J. Wimberley,[60] M. A. Winn,[7] J. Wishahi,[10] W. Wislicki,[29] M. Witek,[27] G. Wormser,[7] S. A. Wotton,[49] K. Wraight,[53] K. Wyllie,[40] Y. Xie,[65] Z. Xu,[4] Z. Yang,[3] Z. Yang,[60] Y. Yao,[61] H. Yin,[65] J. Yu,[65] X. Yuan,[61] O. Yushchenko,[37] K. A. Zarebski,[47] M. Zavertyaev,[11,c] L. Zhang,[3] Y. Zhang,[7] A. Zhelezov,[12] Y. Zheng,[63] X. Zhu,[3] V. Zhukov,[33] J. B. Zonneveld,[52] and S. Zucchelli[15]

(LHCb Collaboration)

[1]*Centro Brasileiro de Pesquisas Físicas (CBPF), Rio de Janeiro, Brazil*
[2]*Universidade Federal do Rio de Janeiro (UFRJ), Rio de Janeiro, Brazil*
[3]*Center for High Energy Physics, Tsinghua University, Beijing, China*
[4]*LAPP, Université Savoie Mont-Blanc, CNRS/IN2P3, Annecy-Le-Vieux, France*
[5]*Clermont Université, Université Blaise Pascal, CNRS/IN2P3, LPC, Clermont-Ferrand, France*
[6]*CPPM, Aix-Marseille Université, CNRS/IN2P3, Marseille, France*
[7]*LAL, Université Paris-Sud, CNRS/IN2P3, Orsay, France*
[8]*LPNHE, Université Pierre et Marie Curie, Université Paris Diderot, CNRS/IN2P3, Paris, France*
[9]*I. Physikalisches Institut, RWTH Aachen University, Aachen, Germany*
[10]*Fakultät Physik, Technische Universität Dortmund, Dortmund, Germany*
[11]*Max-Planck-Institut für Kernphysik (MPIK), Heidelberg, Germany*
[12]*Physikalisches Institut, Ruprecht-Karls-Universität Heidelberg, Heidelberg, Germany*
[13]*School of Physics, University College Dublin, Dublin, Ireland*
[14]*Sezione INFN di Bari, Bari, Italy*
[15]*Sezione INFN di Bologna, Bologna, Italy*
[16]*Sezione INFN di Cagliari, Cagliari, Italy*
[17]*Università e INFN, Ferrara, Ferrara, Italy*
[18]*Sezione INFN di Firenze, Firenze, Italy*
[19]*Laboratori Nazionali dell'INFN di Frascati, Frascati, Italy*

[20]*Sezione INFN di Genova, Genova, Italy*
[21]*Università & INFN, Milano-Bicocca, Milano, Italy*
[22]*Sezione INFN di Milano, Milano, Italy*
[23]*Sezione INFN di Padova, Padova, Italy*
[24]*Sezione INFN di Pisa, Pisa, Italy*
[25]*Sezione INFN di Roma Tor Vergata, Roma, Italy*
[26]*Sezione INFN di Roma La Sapienza, Roma, Italy*
[27]*Henryk Niewodniczanski Institute of Nuclear Physics Polish Academy of Sciences, Kraków, Poland*
[28]*AGH - University of Science and Technology,
Faculty of Physics and Applied Computer Science, Kraków, Poland*
[29]*National Center for Nuclear Research (NCBJ), Warsaw, Poland*
[30]*Horia Hulubei National Institute of Physics and Nuclear Engineering, Bucharest-Magurele, Romania*
[31]*Petersburg Nuclear Physics Institute (PNPI), Gatchina, Russia*
[32]*Institute of Theoretical and Experimental Physics (ITEP), Moscow, Russia*
[33]*Institute of Nuclear Physics, Moscow State University (SINP MSU), Moscow, Russia*
[34]*Institute for Nuclear Research of the Russian Academy of Sciences (INR RAN), Moscow, Russia*
[35]*Yandex School of Data Analysis, Moscow, Russia*
[36]*Budker Institute of Nuclear Physics (SB RAS), Novosibirsk, Russia*
[37]*Institute for High Energy Physics (IHEP), Protvino, Russia*
[38]*ICCUB, Universitat de Barcelona, Barcelona, Spain*
[39]*Universidad de Santiago de Compostela, Santiago de Compostela, Spain*
[40]*European Organization for Nuclear Research (CERN), Geneva, Switzerland*
[41]*Institute of Physics, Ecole Polytechnique Fédérale de Lausanne (EPFL), Lausanne, Switzerland*
[42]*Physik-Institut, Universität Zürich, Zürich, Switzerland*
[43]*Nikhef National Institute for Subatomic Physics, Amsterdam, The Netherlands*
[44]*Nikhef National Institute for Subatomic Physics and VU University Amsterdam,
Amsterdam, The Netherlands*
[45]*NSC Kharkiv Institute of Physics and Technology (NSC KIPT), Kharkiv, Ukraine*
[46]*Institute for Nuclear Research of the National Academy of Sciences (KINR), Kyiv, Ukraine*
[47]*University of Birmingham, Birmingham, United Kingdom*
[48]*H.H. Wills Physics Laboratory, University of Bristol, Bristol, United Kingdom*
[49]*Cavendish Laboratory, University of Cambridge, Cambridge, United Kingdom*
[50]*Department of Physics, University of Warwick, Coventry, United Kingdom*
[51]*STFC Rutherford Appleton Laboratory, Didcot, United Kingdom*
[52]*School of Physics and Astronomy, University of Edinburgh, Edinburgh, United Kingdom*
[53]*School of Physics and Astronomy, University of Glasgow, Glasgow, United Kingdom*
[54]*Oliver Lodge Laboratory, University of Liverpool, Liverpool, United Kingdom*
[55]*Imperial College London, London, United Kingdom*
[56]*School of Physics and Astronomy, University of Manchester, Manchester, United Kingdom*
[57]*Department of Physics, University of Oxford, Oxford, United Kingdom*
[58]*Massachusetts Institute of Technology, Cambridge, MA, United States*
[59]*University of Cincinnati, Cincinnati, OH, United States*
[60]*University of Maryland, College Park, MD, United States*
[61]*Syracuse University, Syracuse, NY, United States*
[62]*Pontifícia Universidade Católica do Rio de Janeiro (PUC-Rio), Rio de Janeiro, Brazil, associated to
Universidade Federal do Rio de Janeiro (UFRJ), Rio de Janeiro, Brazil*
[63]*University of Chinese Academy of Sciences, Beijing, China, associated to Center for High Energy
Physics, Tsinghua University, Beijing, China*
[64]*School of Physics and Technology, Wuhan University, Wuhan, China, associated to Center for High
Energy Physics, Tsinghua University, Beijing, China*
[65]*Institute of Particle Physics, Central China Normal University, Wuhan, Hubei, China, associated to
Center for High Energy Physics, Tsinghua University, Beijing, China*
[66]*Departamento de Fisica, Universidad Nacional de Colombia, Bogota, Colombia, associated to LPNHE,
Université Pierre et Marie Curie, Université Paris Diderot, CNRS/IN2P3, Paris, France*
[67]*Institut für Physik, Universität Rostock, Rostock, Germany, associated to Physikalisches Institut,
Ruprecht-Karls-Universität Heidelberg, Heidelberg, Germany*
[68]*National Research Centre Kurchatov Institute, Moscow, Russia, associated to Institute of Theoretical
and Experimental Physics (ITEP), Moscow, Russia*
[69]*National Research Tomsk Polytechnic University, Tomsk, Russia, associated to Institute of Theoretical
and Experimental Physics (ITEP), Moscow, Russia*

[70]Instituto de Fisica Corpuscular, Centro Mixto Universidad de Valencia - CSIC, Valencia, Spain, associated to ICCUB, Universitat de Barcelona, Barcelona, Spain
[71]Van Swinderen Institute, University of Groningen, Groningen, The Netherlands, associated to Nikhef National Institute for Subatomic Physics, Amsterdam, The Netherlands

[†]Deceased.
[a]Universidade Federal do Triângulo Mineiro (UFTM), Uberaba-MG, Brazil.
[b]Laboratoire Leprince-Ringuet, Palaiseau, France.
[c]P.N. Lebedev Physical Institute, Russian Academy of Science (LPI RAS), Moscow, Russia.
[d]Università di Bari, Bari, Italy.
[e]Università di Bologna, Bologna, Italy.
[f]Università di Cagliari, Cagliari, Italy.
[g]Università di Ferrara, Ferrara, Italy.
[h]Università di Genova, Genova, Italy.
[i]Università di Milano Bicocca, Milano, Italy.
[j]Università di Roma Tor Vergata, Roma, Italy.
[k]Università di Roma La Sapienza, Roma, Italy.
[l]AGH - University of Science and Technology, Faculty of Computer Science, Electronics and Telecommunications, Kraków, Poland.
[m]LIFAELS, La Salle, Universitat Ramon Llull, Barcelona, Spain.
[n]Hanoi University of Science, Hanoi, Viet Nam.
[o]Università di Padova, Padova, Italy.
[p]Università di Pisa, Pisa, Italy.
[q]Università degli Studi di Milano, Milano, Italy.
[r]Università di Urbino, Urbino, Italy.
[s]Università della Basilicata, Potenza, Italy.
[t]Scuola Normale Superiore, Pisa, Italy.
[u]Università di Modena e Reggio Emilia, Modena, Italy.
[v]Iligan Institute of Technology (IIT), Iligan, Philippines.
[w]Novosibirsk State University, Novosibirsk, Russia.